# Residual Stress Maps Determination with global Digital Image Correlation

Théo Jovani, Hélène Chanal, Benoît Blaysat, Michel Grédiac

Available online at www.sciencedirect.com

ScienceDirect

Procedia CIRP 00 (2022) 000–000

www.elsevier.com/locate/procedia

6th CIRP Conference on Surface Integrity

# Residual Stress Maps Determination with global Digital Image Correlation

Théo Jovani[a,*], Hélène Chanal[a], Benoît Blaysat[a], Michel Grédiac[a]

[a] *Université Clermont Auvergne, Clermont Auvergne INP, CNRS, Institut Pascal, F-63000 Clermont-Ferrand, France*

* Corresponding author. *E-mail address:* theo.jovani@sigma-clermont.fr

**Abstract**

Aeronautic workpieces are produced thanks to heavy processes and undergo heat treatments to exhibit high mechanical properties. These operations generate residual stress within the material which are released during machining steps. Thus, workpieces deform to satisfy the internal equilibrium. The knowledge of residual stress maps of raw materials is an important data to control final part deflection. In this paper, a method relying on global Digital Image Correlation is proposed in order to measure the residual stress distribution and induced deformations during the machining of a specimen. It ensures to measure deformation part fields without unclamping unlike classical methods.



*Keywords:* Residual Stress Maps ; Beam machining ; Global Digital Image Correlation

## 1. Introduction

Aeronautic workpieces must exhibit high mechanical performances. Raw parts are obtained thanks to heavy mechanical processes such as molding and/or forging and then, mostly undergo heat treatments such as quenching. All these processes may induce internal residual stress fields composed of both tensile and compressive stresses combined as a self-balanced distribution under uniform temperature conditions and without external loading [1]. During the machining step, the material removal causes the release of these residual stresses. Thus, workpieces deform to satisfy the internal equilibrium. These deformations are especially high for aeronautic parts due to their size which can be several meters and their removal rate during machining which can be more than 90%.

These deformations represent a major issue for parts manufacturers. Actually, additional operations must be set up in order to rectify the manufactured workpieces. A study led by Boeing on four aircraft programs shows that these operations amount to 290 millions dollars a year [2]. Further more, in the same study is shown that deformations beyond allowed geometrical tolerances have a 47% probability of appearing. Another study highlights that these operations amount to several millions dollars a year for each aeronautic part manufacturer [3]. Consequently, it is essential to know the internal residual stress distribution in order to adapt machining strategies and sequences to control part deflection. Moreover, the development of a method that allows to determine the residual stress map during machining without unclamping may be the first step to propose a way to control part deflection by adapting the machining operations while letting the workpiece clamped on the machine-tool.

Thus, this paper proposes a method to measure part deflections and then to deduce residual stress maps during machining the residual stress map of a raw beam made in Al7075-T6 intended for aeronautic workpieces. This method merges a machining strategy called Layer Removal Method and a non-contact full-field measurement technique called Digital Image Correlation. Unlike classical residual stress maps determination methods, this approach allow to let the workpiece clamped during the machining step.

This work is part of a global project called IMaDe aiming at creating an intelligent machining cell to control the deformations of aeronautical parts during machining. This work is done in collaboration with the French laboratory LaBoMaP.

In this paper, the residual stress determination technique relying on the Layer Removal Method will be firstly exposed. Secondly, the non-contact full-field measurement method called Digital Image Correlation adapted to a machining context will be detailed. Finally, the experimental setup will be presented as well as the retrieved results.

* Corresponding author. *E-mail address:* theo.jovani@sigma-clermont.fr

## 2. Residual stress determination

Different methods exist in order to retrieve initial residual stress maps. They are classified in two categories, direct methods and indirect ones. To name a few, neutron diffraction and crack-compliance methods are one of the most commonly used. However, these methods are restricted to thin components and cannot retrieve residual stress maps within thick parts. For large parts along their thickness, several methods are employed such as sectioning or Layer Removal methods. They are based on the partial or complete destruction of the workpiece. They consist of disturbing the residual stress equilibrium in order to cause part to deform. Then, the resulting deformations are measured and linked to the released residual stresses, allowing to retrieve the initial maps.

The method proposed in this paper is based on the Layer Removal Method which has already proven its efficiency concerning the measurement of initial residual stress maps in thick components [4]. It is based on the removal of thin layers from the top of the part to be characterized. Traditionally, it involves the workpiece to be unclamped from the machine-tool after each layer removal in order to measure the induced part deformation. Then, the initial stress map is successively determined from these measurements. The Layer Removal Method proposed from [5] is adapted to our context. The problem parametrization is presented in Fig. 1.

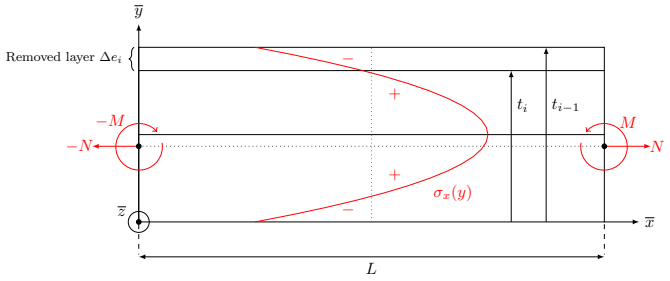


Fig. 1: Layer Removal Method model from the top of the beam to be characterized. The initial residual stress distribution $\sigma_x(y)$ is represented in an arbitrary way.

Only the residual stress distribution along the rolling direction ($\overline{x}$-axis) of the beam is studied. The distribution is supposed to only depend on the part thickness and is represented in a arbitrary way as $\sigma_x(y)$. The beam material is considered isotropic and elastic constants are supposed identical within the material. When a layer of thickness $\Delta e_i$ is machined, the remaining internal residual stresses are reorganized in order to satisfy the internal equilibrium, leading thus the beam to deflect. The stresses within the removed layer are assumed to act as an external load on the remaining part of the beam [5]. This load induces at the beam neutral plane a bending moment $M$ and a normal force $N$. The normal force may be neglected aside the bending moment. Considering Euler-Bernoulli beam theory, the residual stress values are incrementally determined after each layer removal $i$ as follows :

$$\sigma_{x_i} = \frac{\frac{E}{12}\left(t_i^3\gamma_i - t_{i-1}^3\gamma_{i-1}\right) - \frac{1}{2}\Delta e_i \sum_{n=1}^{i-1}\left(\sigma_{x_n}\Delta e_n\right)}{\frac{1}{2}\Delta e_i\left(t_i + \frac{\Delta e_i}{2}\right)} \quad (1)$$

with $E$ the material Young's modulus, $t_i$ and $\gamma_i$ respectively the beam thickness and curvature at the $i^{th}$ step and $\Delta e_i$ the removed layer thickness at the $i^{th}$ step.

Equation (1) allows to retrieve iteratively the residual stress distribution $\sigma_x(y)$. However, it involves the workpiece to be unclamped from the machine-table in order to measure successive part thicknesses and curvatures. The method proposed in this paper intends to let the workpiece clamped. In order to reach this goal, it is assumed that the curvature at the center of the clamped beam is the same as the one of the unclamped beam. Hence, it allows to retrieve the residual stress distribution while letting the workpiece clamped. In order to validate this hypothesis, precautions have been taken with regard to the part positioning and clamping systems. They are detailed in the section dedicated to the experimental setup.

In order to measure the beam displacement fields throughout the machining step and to deduce from them the successive beam central curvatures, Digital Image Correlation (DIC) is employed. The DIC formulation is detailed in the next section.

## 3. Digital Image Correlation during machining

### 3.1. DIC formulation

Digital Image Correlation (DIC) is a non-contact measurement method established in the 80's and is since massively used in experimental mechanics field [6]. It relies on pictures of a specimen undergoing loadings in order to retrieve its displacement fields. Unlike classical measuring systems such as probes or strain gauges, DIC provides full-field measurements and retrieves displacements at any point of the observed surface. The monitored specimen region is defined as Region of Interest (*RoI*) and its contrast is enhanced by painting a speckle onto it.

Hence, taken pictures are composed of pixels associated with gray level values. Considering a reference picture $f$ of the studied specimen, each pixel $P$ coordinates are defined as : $\overline{x_P} = x\overline{x} + y\overline{y}$. The associated gray level value is defined as $f(\overline{x_P})$. The idea is to follow the deformation of the specimen by taking several pictures. Considering another picture $g$, the pixels $P$ are subjected to the displacement field $\overline{u}$ undergone by the specimen. The new associated gray level values are defined as $g(\overline{x_P} + \overline{u}(\overline{x_P}))$. An example of a speckle undergoing a displacement field $\overline{u}$ between two deformation states is presented Fig. (2).

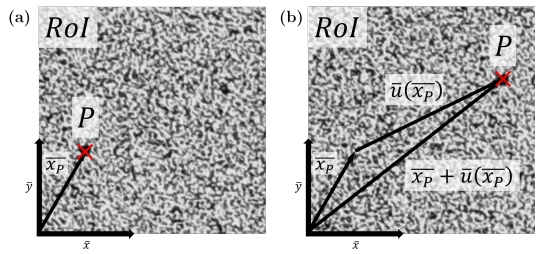


Fig. 2: (a) Speckle region on the reference picture $f$. (b) Same speckle region as (a) on the deformed picture $g$.

DIC is based on the conservation of the surface optical flow between two pictures, which means that the gray level value of each pixel of the *RoI* is preserved. The optical flow conservation is defined as follows [6] :

$$\forall \overline{x_P} \in RoI, \qquad f(\overline{x_P}) - g(\overline{x_P} + \overline{u}(\overline{x_P})) \approx 0 \tag{2}$$

DIC's aim is to retrieve the displacement field $\overline{u}$. Usually, a kinematics space $\mathcal{U}$ is introduced and lies in a linear span composed of a set of $m$ functions $(\overline{\varphi_i})_{1\leq i\leq m}$. Thus, the displacement field is completely described over the *RoI* with $m$ Degrees of Freedom (DoFs) denoted by $(\lambda_i)_{1\leq i\leq m}$ :

$$\overline{u}(\overline{x_P}, \boldsymbol{\lambda}) = \sum_{i=1}^{m} \lambda_i \overline{\varphi_i}(\overline{x_P}) \tag{3}$$

However, because of the presence of metal chips, the camera sensor noise, optical distortions and possible sub-pixel displacements, the optical flow is not correctly preserved between two pictures. Hence, the residual of Eq. (2) is considered and its norm is minimized over the *RoI* with respect to the sought displacement field. This reformulation defines the optimized DoFs :

$$\boldsymbol{\lambda_{opti}} = \underset{\lambda^* \in \Re^m}{\operatorname{argmin}} \left[ \sum_{\overline{x_P} \in RoI} \left( f(\overline{x_P}) - g\left( \overline{x_P} + \sum_{i=1}^{m} \lambda_i^* \overline{\varphi_i}(\overline{x_P}) \right) \right)^2 \right] \tag{4}$$

where $\boldsymbol{\lambda_{opti}}$ is a $m \times 1$ vector containing the optimized DoFs values describing the displacement field $\overline{u}$ minimizing the residual norm between two pictures.

In order to solve Eq. (4), a modified Gauss-Newton scheme is employed, which allows to determine the optimized DoFs $\boldsymbol{\lambda_{opti}}$ by incrementally updating $\boldsymbol{\lambda}$ from an initial guess $\boldsymbol{\lambda^0}$ with the following scheme :

$$\boldsymbol{\lambda}^{k+1} = \boldsymbol{\lambda}^k + \mathbf{M}^{-1} \times \mathbf{L} \times \boldsymbol{\Psi}(\boldsymbol{\lambda}^k) \tag{5}$$

where,

- vector $\boldsymbol{\Psi}(\boldsymbol{\lambda}^k)$ corresponds to the pixels optical residual values,
- matrix $\mathbf{L}$ corresponds to the kinematics functions projected onto the reference image gradient,
- and matrix $\mathbf{M}$ corresponds to the DIC tangent operator, more commonly called correlation matrix.

An interested reader may refer to [7] for detailed calculations of $\boldsymbol{\Psi}$, $\mathbf{L}$ and $\mathbf{M}$. In Eq. (5), the quantity $\mathbf{M}^{-1} \times \mathbf{L} \times \boldsymbol{\Psi}(\boldsymbol{\lambda}^k)$ corresponds to the updated quantity of the DIC algorithm, defined as $\delta\boldsymbol{\lambda}^k$. The convergence criterion of the DIC algorithm is often defined as the value of the Euclidean norm of $\delta\boldsymbol{\lambda}^k$, compared to a threshold value generally chosen equals to $10^{-6}$. In order to iteratively compute the updated quantity, the kinetics space $\mathcal{U}$ must be defined, that means that the shape functions $(\overline{\varphi_i})$ composing it must be chosen.

### 3.2. Shape functions

In Eq. (3), the *RoI* displacement field $\overline{u}$ is defined through a set of $m$ shape functions weighted with their respective DoFs. The chosen set depends on the employed DIC method, which can be local or global. For a local DIC method, a small subset of the whole *RoI* is chosen and simple shape functions are used, relying mostly on rigid-body motion functions. For a global DIC method, the whole *RoI* is chosen as well as advanced shape functions, such as Chebyshev polynomials, finite element functions or NURBS. For this study, a global DIC is employed where the *RoI* matches the entire monitored specimen surface, in order to fully describe the beam displacement field, especially at the specimen ends. The displacement field is defined thanks to shape functions based on the beam elasticity theory.

In Rebergue's study [8], the implementation of DIC to measure part deflection during machining was realized. As the camera was directly mounted on the machine-table, it was subjected to machine vibrations. This study proves the relevancy of choosing two *RoIs* as well as two speckles to differentiate workpiece deformations induced by the machining step from camera movements. In our case, speckles are also applied onto the workpiece monitored surface as well as the workpiece-holder surface as illustrated in Fig. (3).


Fig. 3: *RoIs* and speckles definitions. $RoI_{Ref}$ is used to determine camera rigid-body motion caused by vibrations. $RoI_{Part}$ is used to retrieve beam deflection due to the machining step.

The shape functions are respectively defined to describe the rigid-body motion of the camera caused by machine vibrations ($RoI_{Ref}$) and to describe the beam deflection during machining ($RoI_{Part}$). Hence, the displacement field solely due to the residual stress release $\overline{u_\sigma}$ is expressed using Eq. (3) and is denoted by :

$$\overline{u_\sigma}(\overline{x_P}) = \sum_{i=1}^{m_{Part}} \lambda_{Part_i} \overline{\varphi_{Part_i}}(\overline{x_P}) - \sum_{i=1}^{m_{Ref}} \lambda_{Ref_i} \overline{\varphi_{Ref_i}}(\overline{x_P}) \tag{6}$$

The shape functions referred as $\overline{\varphi_{Ref}}$ and $\overline{\varphi_{Part}}$ are detailed in their respective subsections.

### 3.2.1. Reference shape functions

During machining, as camera is directly mounted on the machine-table, it is subjected to machining vibrations which cause the pictures to have a different framing. The camera displacement field between two loading states is described using the whole picture. The four corners of the picture define the nodes of a quad4-isogeometric element. In order to retrieve the camera motion between two loading states, a DIC algorithm is applied onto $RoI_{Ref}$. The shape functions $\overline{\varphi_{Ref}}$ used to describe the camera motion correspond to the linear interpolation of the quad4-isogeometric element nodes, as described in Eq. (7). Rigid-body motion as well as first order strain are totally described, hence fully describing possible expected camera movements.

$$\overline{\varphi_{Ref}}(\overline{x_P}) = \frac{1}{4}\left(1 \pm \left(\frac{2x}{a} - 1\right)\right)\left(1 \pm \left(\frac{2y}{b} - 1\right)\right) \tag{7}$$

where, $(a, b)$ are the picture dimensions respectively along the $\overline{x}$- and $\overline{y}$-axis.

### 3.2.2. Part shape functions

In order to determine the workpiece displacement field during machining, a DIC algorithm is applied onto $RoI_{Part}$. The implemented shape functions set shall describe a displacement field corresponding to a beam-like deflection. A finite element method is employed here to describe the beam geometry as well as to define the shape functions. The used approach consist of dividing the beam into several 2D-beam elements $k$. Each 2D-beam element includes two nodes whose have three DoFs each, as described in Fig. (4).

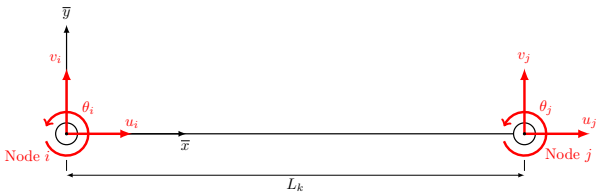


Fig. 4: 2D-beam element used to discretize the workpiece.

Each 2D-beam element is supposed to satisfy Euler-Bernoulli conditions. For a material point of a beam cross-section whose initial coordinates are $(x, y)$, its displacement field $[u_{Part}\ v_{Part}]^T$, along $\overline{x}$- and $\overline{y}$-axis, is defined with respect to the 2D-beam element DoFs and geometry. Its displacement field is expressed using a shape functions matrix denoted by $\mathbf{N_k}$ and is given in Eq. (8) [9].

$$\begin{bmatrix} u_{Part} \\ v_{Part} \end{bmatrix} = \begin{bmatrix} 1-\xi & 0 \\ 6\eta(\xi-\xi^2) & 1-3\xi^2+2\xi^3 \\ L_k\eta(-1+4\xi-3\xi^2) & L_k\xi(1-2\xi+3\xi^2) \\ \xi & 0 \\ 6\eta(\xi^2-\xi) & \xi^2(3-2\xi) \\ L_k\eta(-3\xi^2+2\xi) & L_k\xi^2(\xi-1) \end{bmatrix}^T \begin{bmatrix} u_i \\ v_i \\ \theta_i \\ u_j \\ v_j \\ \theta_j \end{bmatrix} \tag{8}$$

where, $\xi = \dfrac{x}{L_k}$ and $\eta = \dfrac{y}{L_k}$.

The terms of the matrix $\mathbf{N_k}$ correspond to the shape functions describing the displacement field of a point from the $k^{th}$ 2D-beam element.

In our case, the workpiece is horizontally divided into 15 2D-beam elements. Thus, the sought shape functions $\overline{\varphi_{Part}}$ in Eq. (6) are expressed as follows :

$$\overline{\varphi_{Part}}(\overline{x_P}) = [\mathbf{N_1}, ..., \mathbf{N_k}] \tag{9}$$

The DoFs $\boldsymbol{\lambda_{Part}}$ used to weight the shape functions $\overline{\varphi_{Part}}$ correspond consequently to the nodal DoFs of the 15 2D-beam elements.

## 4. Experimental setup

The method proposed in this paper has been applied to a Al7075-T6 aluminum-alloy beam of dimensions $200 \times 99 \times 40\,\text{mm}^3$. 60 layers of a thickness $e = 0.5$ mm have been successively machined from the top surface of the beam using a 5-axe CRENO HSM (High-Speed Machining) machine-tool of nominal power 12 kW, equipped with an electrospindle HSD ES799. The successive milling operations have been realized thanks to a Sandvik R590-110504H-NL H10 D100 milling cutter with six Sandvik R590-110504H-NL H10 inserts mounted on a HSK 63F tool-holder. The cutting parameters are presented in the Table 1. Between each milling operation, a cooling time of 5 minutes is set so that the workpiece is allowed to reach ambient temperature. Fig. (5) depicts the machined beam before and after the machining procedure.

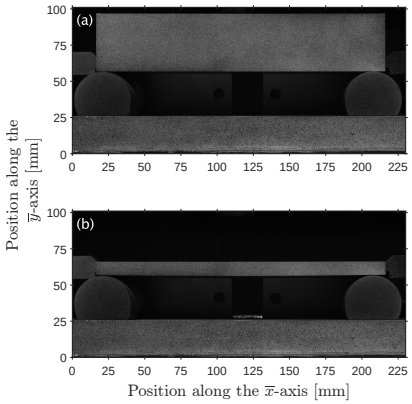


Fig. 5: (a) Workpiece before machining. (b) Workpiece after the machining of 60 layers.

Table 1: Cutting parameters with $D$ diameter ($mm$), $Z$ number of teeth, $V_c$ cutting speed (m.min$^{-1}$), $f_z$ feed rate per tooth (mm.r$^{-1}$.teeth$^{-1}$), $V_f$ feed rate (mm.min$^{-1}$), $a_p$ depth of cut (mm) and $N$ spindle speed (r.min$^{-1}$).

| Tool | D | $Z$ | $V_c$ | $f_z$ | $V_f$ | $a_p$ | $N$ |
|---|---|---|---|---|---|---|---|
| Milling cutter | 100 | 6 | 1000 | 0.1 | 1911 | 1 | 3183 |

Concerning the positioning system as well as the clamping system, precautions have been taken in order to let the workpiece free to deform while machining. The goal was to minimize the effect of the clamping system on the beam deflection and to measure beam curvature while letting it clamped. Indeed, Cherif has shown that the clamping system has a significant impact on the workpiece deviation when internal residual stress are released [10]. When the clamping system is too restrictive, the workpiece cannot deform sufficiently to restore the internal equilibrium, causing the workpiece to deflect more as it is unclamped. In our case, the workpiece has been raised at its ends thanks to two semi-cylindrical wedges in order to minimize the support area underneath the workpiece. Also, this configuration enables the beam to freely deform upwards on downwards at its middle area. Workpiece was also positioned on its back surface thanks to a straight line and was fixed on the machine-table thanks to two flanges inserted into two dedicated sloths at both beam ends. The clamping has been controlled thanks to a torque wrench at 60 N.m, leading to a 10 kN effort on each sloth. The workpiece mounting setup is depicted in Fig. (6) and (7).

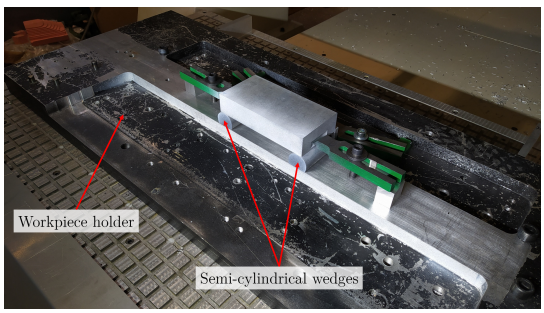


Fig. 6: Workpiece mounting setup (front view).

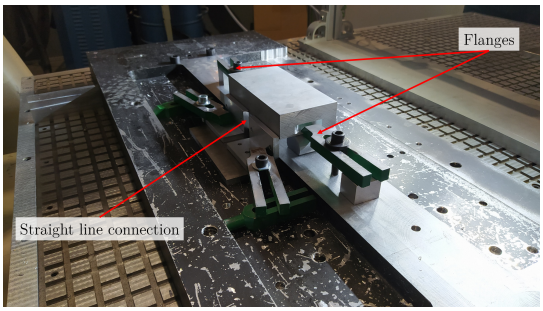


Fig. 7: Workpiece mounting setup (back view).

61 pictures have been taken with a Prosilica GT-6600 camera equipped with a EX SIGMA 105 mm F2.8 DG Macro lens and also with a 5-DSR Canon camera equipped with a TAMRON 90 mm F2.8 Di MACRO 1:1 VC USD lens. Cameras were directly clamped on the machine-table thanks to a dedicated support. The monitored surface was lighted thanks to a dedicated lighting system which was also mounted on the machine-table. The experimental setup is illustrated Fig. (8).

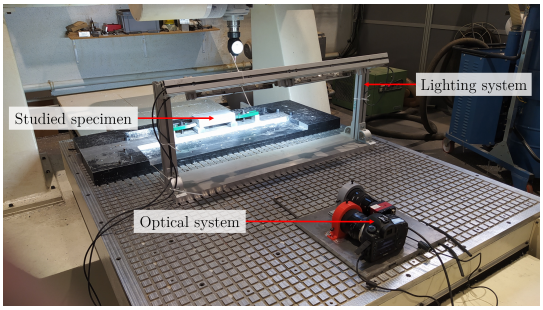


Fig. 8: Experimental setup.

## 5. Results

The beam displacement field $\overline{u_\sigma}$ along the $\overline{x}-$ and $\overline{y}-$ axis solely due to the residual stress release is retrieved using Eq. (6). Each term composing $\overline{u_\sigma}$ is determined thanks to a global DIC algorithm applied onto $RoI_{Ref}$ and onto $RoI_{Part}$, as described in section (3). As the beam curvature is used to determine the initial residual stress map (see Eq. (1)), only the successive neutral fiber deflections of the beam are retrieved. Fig. (9) illustrates the position of the beam neutral fiber throughout the machining step.

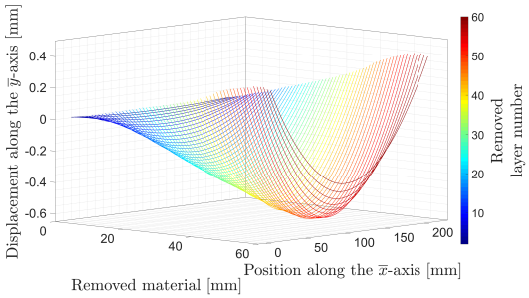


Fig. 9: Evolution of the beam neutral fiber deflection throughout the machining procedure.

Curvature is then calculated for each deflection at the beam center. After each curvature calculation, a point of the initial residual stress map is computed thanks to Eq. (1). The obtained residual stress map is illustrated in Fig. (10). The retrieved map is also compared to the one identified by Louhichi from LaBoMaP, the other laboratory participating in the IMaDe project. The traditional Layer Removal Method was here realized on a beam specimen with the same dimensions and composed of the same aluminum-alloy. Comparing the two obtained curves, the method proposed in this paper seems to determine a similar initial residual stress map. There are a compressive stress underneath both beam surfaces (from 0 mm to 10 mm and from 30 mm to 40 mm) and a tensile stress in the core part of the beam (from 10 mm to 30 mm). The trend of the curve follows also the one determined with the traditional Layer Removal Method. Indeed, it is relevant to note that magnitude values on both curves are close with a minimum value at 165 MPa and a maximum value at 75 MPa.

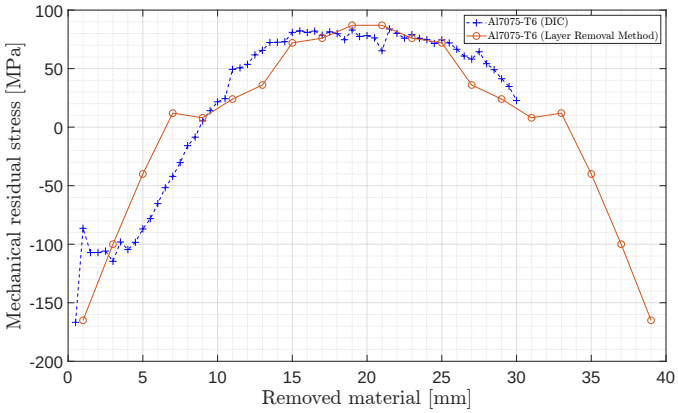


Fig. 10: Residual stress maps comparison. Blue curve is the one retrieved by DIC while letting the workpiece clamped. Red curve is the one retrieved thanks to traditional Layer Removal Method realized by Louhichi from LaBoMaP.

## 6. Conclusion

This paper describes a novel approach to account for the effect of residual stresses on the geometry of a workpiece being milled. The proposed method merges a measuring technique employed to determine residual stress maps within thick components called Layer Removal Method and a non-contact full-field measuring method called global Digital Image Correlation. Using predictive deformations models, this method allows to determine the displacement fields of a beam being machined and to retrieve the initial residual stress map within the material. Contrary to classical residual stress determination methods, the major advantage of the proposed one herein relies on letting the studied specimen clamped during machining. Also, letting the workpiece clamped during machining would further allow to determine the initial residual stress map of a part and then to adapt in real time the machining strategies to control the deformations due to residual stress release.

The residual stress map retrieved thanks to this method has been compared to results obtained by the traditional Layer Removal Method. Curve trend and magnitude values are close which validate the method. Further works are in progress to adapt this method to a three-dimensional measurement and also to retrieve bi-axial residual stress maps.

## Acknowledgements

The authors are grateful to the French National Agency (ANR) for their financial support (IMaDe project, N°ANR-19-CE10-0002-02).

## References

[1] Chandra, U., Das, S., 2003. *Handbook of Aluminium : Physical Metallurgy and Processes*, Volume 1, Springer.

[2] Bowden, D.M., Halley, J.E., 2001. Aluminium reliability improvement program-final report 60606. Chicago, IL, USA: The Boeing Company.

[3] Lequeu, P., Lassince, P., Warner, T. Raynaud, G.M., 2001. Engineering for the future: weight saving and cost reduction initiatives. Aircraft Engineering and Aerospace Technology: An International Journal, Volume 73, Number 2, 2001, pp.147-159(13). 10.1108/00022660110386663.

[4] Aurrekoetxea, M., Bilkhu, R., Llanos, I., Ayvar-Soberanis, S., Norberto, L., Lacalle, L., 2021. Residual stress characterization for ribbed geometries using On-machine Layer Removal method. Procedia CIRP 2021, Volume 101, pp.42-45. 10.1016/j.procir.2020.10.003

[5] Hospers, F., Vogelesang, L.B., 1975. Determination of residual stresses in aluminum-alloy sheet material. Experimental Mechanics, 15:107–110.

[6] Sutton, M.A., Orteu, J.J., Schreier, H., 2009. Image Correlation for Shape, Motion and Deformation Measurements. Springer. pp.1-37. 10.1007/978-0-387-78747-3.

[7] Blaysat, B., Neggers, J., Grédiac, M., Sur, F., 2020. Towards Criteria Characterizing the Metrological Performance of Full-field Measurement Techniques: Application to the Comparison Between Local and Global Versions of DIC. Experimental Mechanics, Society for Experimental Mechanics, 2020, 60 (3), pp.393-407. 10.1007/s11340-019-00566-4.

[8] Rebergue, G., Blaysat, B., Chanal, H., Duc, E., 2022. In-situ measurement of machining part deflection with Digital Image Correlation. Measurement, Volume 187. 10.1016/j.measurement.2021.110301.

[9] Bazoune, A., Khulief, YA., Stephen, NG., 2003. Shape functions of three-dimensional Timoshenko beam element. Journal of Sound and Vibration, 259(2):473–480, 2003. 10.1006/jsvi.2002.5122.

[10] Cherif, I., Cotton, D., Poulachon, G., Outeiro, J., Brosse, A., Rebelo Kornmeier, J., 2019. International Journal of Advanced Manufacturing Technology, Springer Verlag, 2019, 105 (7-8), pp.3093-3103. 10.1007/s00170-019-04510-7.